Journal of Alloys and Compounds 655 (2016) 327–335

Contents lists available at ScienceDirect

Journal of Alloys and Compounds

journal homepage: http://www.elsevier.com/locate/jalcom

Strain dependence of the physical properties of epitaxial $La_{0.7}Ca_{0.3}MnO_3$ thin films grown on $LaAlO_3$ substrates

S. El Helali [a, *], K. Daoudi [b, c], M. Boudard [d], A. Schulman [d, e], C. Acha [e], H. Roussel [d, e], M. Oumezzine [a], M. Oueslati [b]

[a] Laboratoire de Physico-Chimie des Matériaux, Faculté des Science de Monastir, University of Monastir, 5018 Monastir, Tunisia
[b] Unité Nanomatériaux et Photonique, Faculté des Sciences de Tunis, Tunis El Manar University, 2092 El-Manar Tunis, Tunisia
[c] Department of Applied Physics, College of Sciences, University of Sharjah, P.O. Box 27272, Sharjah, United Arab Emirates
[d] LMGP, Univ. Grenoble Alpes, CNRS, Grenoble F-38000, France
[e] Departamento de Física, FCEyN, UBA and IFIBA, Conicet, Pabellón 1, Ciudad Universitaria, 1428 Buenos Aires, Argentina

ARTICLE INFO

Article history:
Received 28 March 2015
Received in revised form
27 August 2015
Accepted 14 September 2015
Available online 15 September 2015

Keywords:
LCMO
Strain
Transport properties
Colossal magnetoresistance

ABSTRACT

We present a systematic study of the structural, magnetic, electrical and magnetoresistive properties of $La_{0.7}Ca_{0.3}MnO_3$ thin films epitaxially grown on $LaAlO_3$ single crystalline substrates using metal organic deposition process. The evolutions of the lattice parameters and the corresponding strain as a function of the film thickness (20–80 nm) have been investigated using X-ray diffraction measurements. The films were found to be totally relaxed for a thickness around 60 nm. Magnetization and resistance measurements as a function of temperature revealed a direct correlation of the transition temperature from a ferromagnetic state to the paramagnetic state with the film thickness. The temperature dependence of the resistivity (ρ (T)) has been fitted using various theoretical approaches. Below the transition temperature (T_P) the ρ (T) graphs were well fitted using the $\rho(T) = \rho_0 + AT^{\alpha}$ formula, in which the fitting parameters ρ_0 and α have been used to clarify the conduction mechanism. Above T_P the ρ (T) graphs were found to be well fitted using different models including the VRH model and the small polaron model. A magnetoresistance of 91% was measured at 248 K for the for 60 nm thick film under an applied magnetic field of 7 T. As well as a non-volatile resistive switching capacity of 15% on Ag contacts deposited on top of this film.

1. Introduction

The perovskite manganite $La_{1-X}A_XMnO_3$ (A = Alkaline earth) have attracted considerable attention because of their unusual magnetic and transport behaviors such as colossal magnetoresistance (CMR) [1,2]. These materials are characterized by a rich and complex phase diagram caused by the competition among spin, charge, orbital and lattice degree of freedom [3,4]. The $La_{1-X}Ca_XMnO_3$ in the doping levels $0.25 < x < 0.33$ shows a CMR characteristics combining simultaneous metal-insulator (MI) and ferromagnetic–paramagnetic (FP) transition [5,6] in temperature $200\ K < T_P < 300\ K$. Also, these materials are known by a large coefficient temperature (TCR) [7]. This makes them key materials for magnetic random access memories, magnetic sensors, and various spintronics devices [8]. Moreover, interfaces made of these materials (as well as other perovskite oxides) with a metal have shown non-volatile and reversible resistance properties, making them suitable to perform resistive random access memories (RRAM) [9,10].

In bulk material, physical properties are correlated to alkaline site which modify the Mn^{3+} to Mn^{4+} and in turn will affect the structure of the coupled system MnO_6 octahedra [11]. Furthermore, in thin film form, these intrinsic physical properties can be affected by the growth method, the deposition parameters and also the substrate-induced strain [12,13].

We recently investigated the transport properties dependence on the substrate material [14]. The LCMO having a thickness of 40 nm have been epitaxially grown on single crystalline $LaAlO_3$ (LAO), $SrTiO_3$ (STO) and $(LaAlO_3)_{0.3}$–$(SrAlTaO_6)_{0.7}$ (LSAT) substrates imposing various strain states. The conduction mechanism is found to be strongly dependent on the lattice mismatch between the film and the used substrate.

* Corresponding author.
E-mail address: saoussen_elhelali@yahoo.fr (S. El Helali).

http://dx.doi.org/10.1016/j.jallcom.2015.09.121
0925-8388/

In this paper we extended our investigation on the effect of the film thickness on the structural, magnetic and electrical transport properties of the LCMO films grown on LAO substrates. The strain is systematically varied by increasing the film thickness from 20 to 80 nm. The structural parameters of the LCMO films have been extracted from the XRD measurements and used to quantitatively determine the evolution of the strain as a function of the film thickness. We present also the correlations between the structural properties and the corresponding, magnetic, electrical transport and magneto-resistance as a function of the induced strain in the films. Additionally, we show the capacity of our films to act as a RRAM memory device based on the resistive switching mechanism.

2. Experimental details

LCMO films were deposited on LAO (001) single crystal substrate using the metal organic deposition (MOD) process [15]. The starting solution was prepared by a mixing constituent metal-naphthenate solution (Nihon Kagaku Sangyo) and diluting with toluene to obtain the required concentration and viscosity. The molar ratios of La, Ca and Mn in the coating solution were 0.7, 0.3 and 1.0, respectively. This solution was spin-coated onto LAO (001) substrate at 4000 rpm for 10 s. To eliminate the toluene, the metal-organic (MO) film was then dried in air at 100 °C for 10 min. Before the final annealing, a preheating step at 500 °C for 30 min is necessary to decompose the organic part. This preheating step is also required to prevent the formation of fissures on the film surface during the final annealing at a high temperature. To obtain a satisfactory film thickness, the above procedure (coating, drying, and preheating) was repeated several times giving rise to a corresponding number of superimposed layers in the LCMO product film. The final annealing was carried out in a conventional furnace at 900 °C for 60 min in air.

Phase purity and film crystallinity were examined by X-ray diffraction (XRD) in Bragg–Brentano geometry using a BRUKER D8 advance diffractometer with monochromatic $CuK_{\alpha 1}$ radiation ($\lambda = 0.154060$ nm) and LynxEye 1 dimension detector. Reciprocal space mappings (RSM) were collected with a RIGAKU Smartlab equipped with a Cu rotating anode (9 kW). An incident high resolution setting was used (1D parabolic mirror and a two-crystal Ge monochromator in the 400 setting) leading to a monochromatic parallel x-ray beam ($CuK\alpha_1$). Optics used after the sample, were two 1.0 mm cross 10.0 mm slits, 2.5° sollers slits and a punctual scintillation counter detector.

Electrical transport measurements were performed using a four-probe technique. Magnetic characterization was performed using a commercial SQUID magnetometer (Quantum Design, 5T) with an applied magnetic field of 500 Oe in both the field cooled (FC) and zero field cooled (ZFC) measurements in the 5–300 K temperature range. We also performed resistive switching hysteresis loop measurements (RSHL), which is a way to test the capacity of a device to act as a memory device. This protocol is useful to characterize the response of the remnant resistance of a device to the amplitude of the applied pulses. The resistance of the LCMO/Ag interface is measured (read operation) after applying current pulses (write operation) of 10 ms following a loop sequence: Iini → Imax → Imin → Iini.

3. Results and discussion

3.1. Structural properties

Fig. 1 shows the θ–2θ XRD patterns around the *002* Bragg reflections of the LCMO films, with different thicknesses ranging from

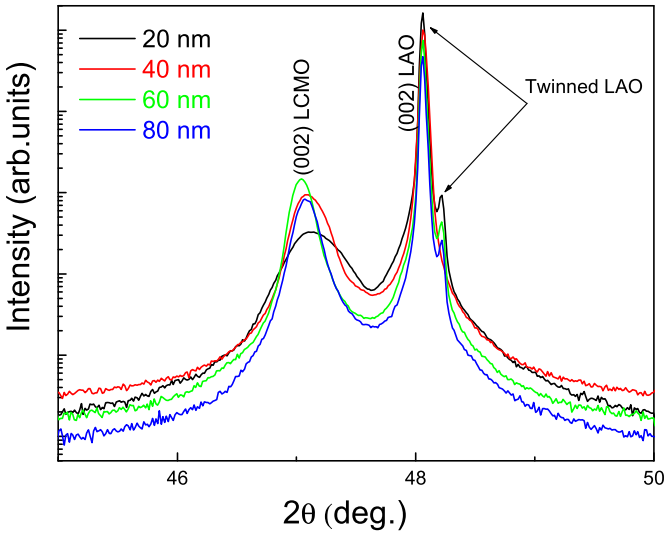

Fig. 1. θ–2θ XRD scans of the LCMO films grown on LAO substrates for different thicknesses.

20 to 80 nm (measured using transmission electron microscopy observations on cross-sections in our previous studies [15]). The LCMO crystallizes into an orthorhombic structure with Pnma symmetry. It is often represented by a pseudo-cubic lattice parameter of 3.858 Å. The lattice parameter of the LAO in the cubic structure is 3.789 Å imposing therefore, an in-plane compressive strain and an out-of-plane compressive strain of 1.84%. The LCMO films grow epitaxially on top of the LAO substrate with common (*00l*) planes orientations (parallels to the surface) i.e. with $[001]_{LCMO}//[001]_{LAO}$ orientation relationship. The splitting of the *002* Bragg peaks of the LAO is due to twinning. By increasing the film thickness from 20 to 80 nm we notice in Fig. 1 some obvious changes in the intensity, the position and the width of the *002* peaks of the LCMO film. The increase in the peak intensity is expected since we increased the quantity of the diffracting material by increasing the film thickness. The *002* LCMO peak is shifted toward lower angles and this correspond to an increase in the out-of-plane parameter "*c*". The out-of-plane lattice parameters have been determined from the θ–2θ XRD scans. Using the "c" parameter, we can extracted the out-of-plane epitaxial strain which can be calculated by the following relation: $\varepsilon_{zz} = (c - c_b)/c_b$, where $\boldsymbol{c}$ is the out-of-plane lattice parameter of the film and $\boldsymbol{c_b}$ is the bulk pseudo-cubic lattice parameter of LCMO. These parameters are listed in Table 1.

The 20 nm thick film has an out-of-plane lattice parameter slightly superior to that one of the bulk LCMO. This small value of the lattice parameter is probably due to the large strain, the poor film crystallinity and the oxygen stoichiometry. By increasing the film thickness for 20 to 40 then 60 nm, the lattice parameter is relatively increased. On reaching the 80 nm thick film, the lattice parameter decreases from 3.863 to 3.860 Å. Considering the cell parameter for bulk LCMO $c_b = 3.858$ Å, the obtained values for *c* indicate that the LCMO is under compressive strain. Furthermore,

Table 1
Out-of-plane lattice parameter (*c*) and the corresponding epitaxial strain (ε_{zz}) of the LCMO films grown on LAO substrates for different thicknesses.

LCMO/LAO	20 nm	40 nm	60 nm	80 nm
c (Å)	3.859 ± 10^{-4}	3.861 ± 10^{-4}	3.863 ± 10^{-4}	3.860 ± 10^{-4}
ε_{zz} (%)	0.026	0.078	0.129	0.052

from the evolution of the out-of-plane lattice parameter ***c*** and the epitaxial strain ε_{zz}, we can estimate the critical thickness (d_c) of strain relaxation to be around 60 nm. Our results are similar to those obtained by I. T. Serenkov et al. [13] on LCMO films prepared by pulsed laser deposition (PLD) process on LAO showing a critical thickness around 80 nm for the strain relaxation. A significant peak broadening for the 20 nm thick film is easily observed in comparison with the relatively thick films (Fig. 1). This broadening has been reported previously in epitaxial LCMO and $La_{1-x}Sr_xCoO_3$ thin films and has been attributed to the finite-size effect [16]. By increasing the film thickness from 40 to 80 nm, the peak broadening disappears, indicating an improvement of the crystalline quality of the film. The epitaxial quality of our film is well evidenced in the reciprocal space maps (RSM) around the 002 and 013 reflections shown in Fig. 2 for the films having 20, 60 and 80 nm in thicknesses.

In the c-plane RSM figure (left panel), the 002 LCMO reflections are well aligned with those of the LAO substrate. On the other hand, the film's reflection changes from an elliptic to a circular shape by increasing the film thickness from 20 to 80 nm, indicating an evolution of the strain along the out-of-plane direction. Similar evolution of strain can also be deduced from the 013 reflection of the film with an increase of the thickness. The 20 nm thick film is well strained in the symmetric direction 002 and also in asymmetric direction 013. In general, coherently strained films in which the film and substrate in-plane lattice parameters are identical can be maintained only up to a critical layer thickness, depending on the amount of the misfit. Above, the critical thickness, the strain energy becomes so large that it is then energetically favorable to nucleate interfacial misfit dislocations [15]. The 60 nm thick film is relaxed, but still containing probably some strained zones. The fully

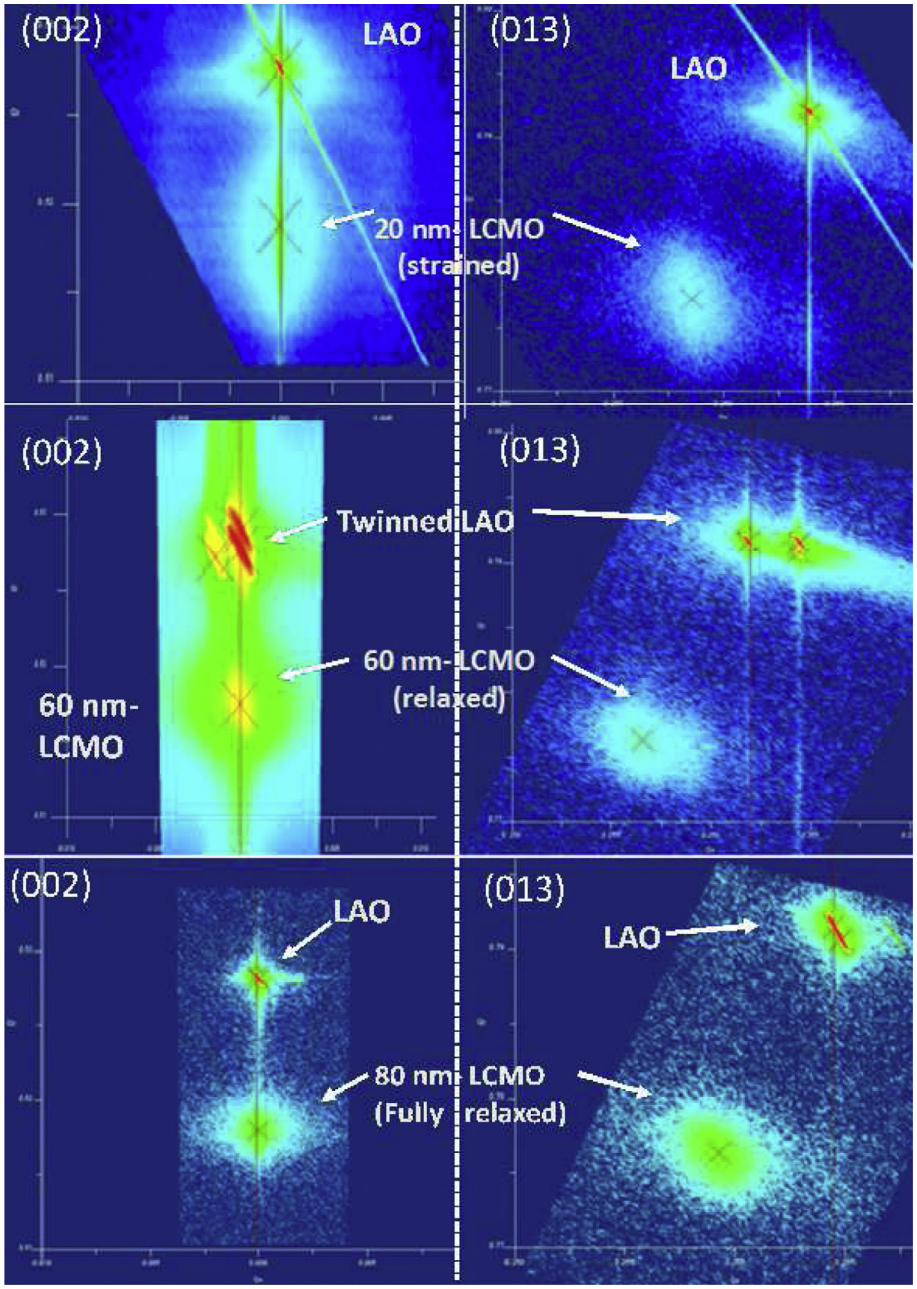

Fig. 2. Reciprocal space mapping for 002(left panel) and 013 (right panel) in pseudocubic type reflections for LCMO/LAO film with different thicknesses (20, 60 and 80 nm).

relaxed film is obtained for a film thickness equal to 80 nm. In these RSM images we can easily distinguish the apparition of twins, especially for the 60 nm thick film.

3.2. Magnetic properties

The temperature dependence of the magnetization (M (T)) for the LCMO films grown on LAO substrates having 20, 40 and 60 nm in thicknesses are shown in Fig. 3. As can be seen, the films of 40 (resp. 60) nm in thicknesses have a saturation magnetization almost two (resp. three) times higher than that of the 20 nm thick film. The 80 nm thick film shows similar magnetization curve (not shown here) to that one exhibited by the 60 nm thick film. All films exhibit a ferromagnetic to paramagnetic transition as T increases. The Curie temperature "T_C" is obtained from the peak in the dM/dT via temperature curve that is shown in inset Fig. 3.

The T_C value increases slightly from 249 K to 253 K by increasing the film thickness from 20 to 40 nm. For the 60 nm thick film, the T_C value decreases and is found to be the same as that for the 20 nm thick film. The decrease in T_C value is due probably to the strain relaxation induced by increasing the film thickness. Bibes et al. [17] studied the effect of the film thickness on the T_C of the LCMO films grown by rf sputtering on STO substrates and found that T_C increases from 100 K to 250 K by increasing the film thickness from 10 nm to 100 nm. Debnath et al. [18] reported almost the same values of T_C in comparison to our LCMO films for a 200 nm thick $La_{0.8}Ca_{0.2}MnO_3$ thin film grown by PLD process on LAO substrate. The 60 nm thick film, which is more relaxed compared to the 40 nm thick film, but do not reach that one of the bulk material ($T_{C,bulk} = 270$ K) [8]. Regardless the film thickness, all films are still under a biaxial strain which induces an increase in the Jahn–Teller distortion will lead to a localization of electrons and reduce Tc [19].

3.3. Electrical transport properties

The electrical transport properties of the LCMO films were investigated as a function of the film thickness and temperature. Fig. 4 (a) shows the zero-field resistivity vs. temperature curves for the LCMO films grown on LAO substrates with various thicknesses (20, 40 and 60 nm). All films exhibit a ferromagnetic –metallic (FM) to paramagnetic-insulator (PI) transitions at the temperature T_P. The electrical resistivity plots of the 20 and 40 nm thick are almost the same throughout the temperature range [5–300 K] with a very

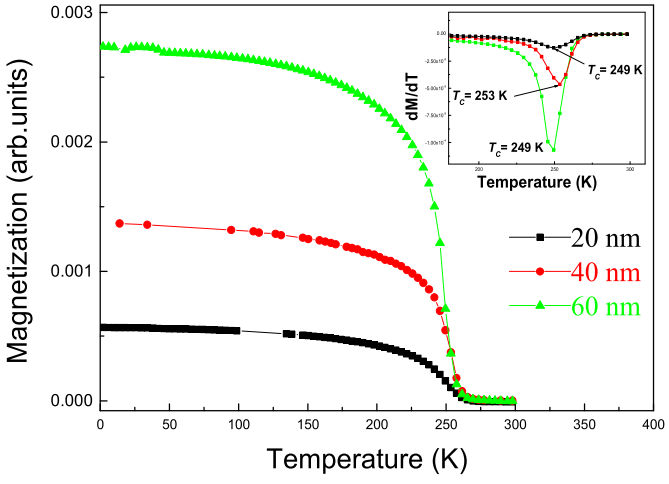

Fig. 3. Temperature dependence of the Magnetization (M –T curves) for the LCMO thin films having different thicknesses (20–40 and 60 nm). The inset shows the dM/dT versus T used for the determination of T_C.

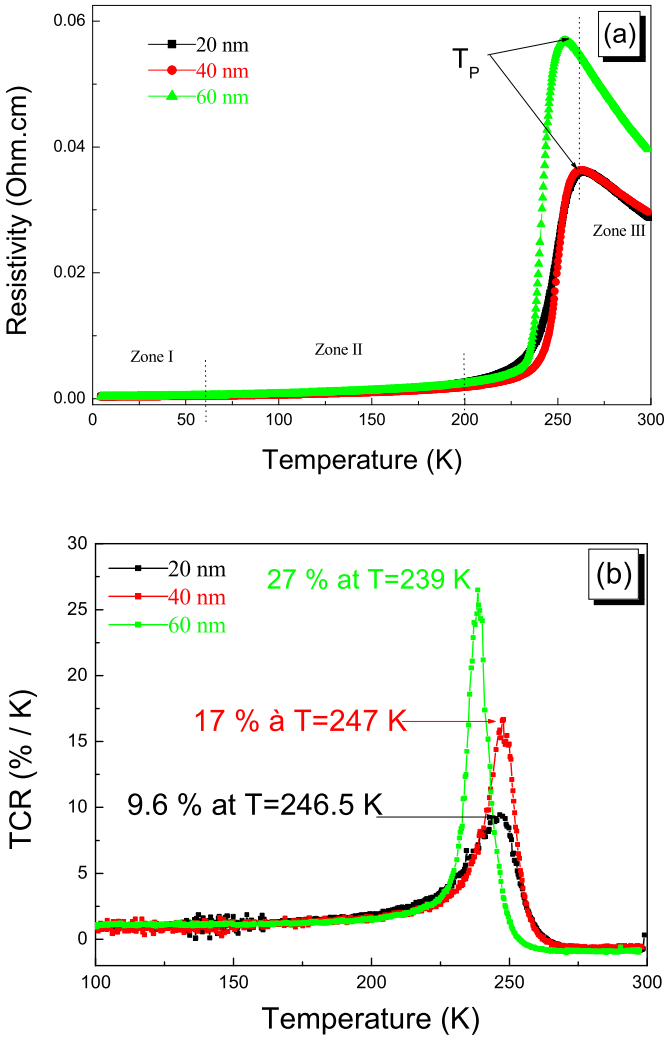

Fig. 4. Temperature dependence of resistivity (a) and *TCR* (b) for the LCMO films grown on LAO substrates with different thickness 20, 40, and 60 nm.

small variation in the transition temperature (T_P). We notice also that the resistivity curve (ρ (T)) becomes sharper for 60 nm thickness and is accompanied with a smallest transition width which T_P decreases. The 80 nm thick film exhibit electrical transport properties (not shown here) similar to those of the 60 nm thick film.

The T_P and T_C values are shown in Table 2. We notice that the transition temperature T_P values are larger than the T_C. Also the T_C values which increases slightly and then decreases with increasing film thickness from 40 to 60 nm, but the T_P values decrease slightly by increasing the film thickness. This dependence of T_P values with the evolution of the film thickness is in a good agreement with several works [20,21].

The lanthanum manganite films have been considered as promising candidates for bolometric applications [22]. High value of the temperature coefficients of resistance defined as TCR(%) = 1/

Table 2
T_C, T_P, T_m and *TCR* parameters for LCMO/LAO films.

LCMO/LAO	20 nm	40 nm	60 nm
T_C (K)	249	253	249
T_P (K)	264	263	254
T_m (K)	246.5	247	239
TCR (%/K)	9.6	17	27

ρ (dρ/dT) × 100 gives high sensitivity of the bolometric device. In this study, we show in Fig. 4 (b) the TCR as a function of temperature of the LCMO films for different thickness (20, 40 and 60 nm). As can be seen the temperature dependence of the TCR is similar to the ρ (T) dependence exhibiting a FM to PI transition at a critical temperature (T_m). The TCR values are summarized in Table 2. The maximum values of TCR are 9.6%K^{-1} at T_m = 246.5 K, 17%K^{-1} at T_m = 247 K and 27%K^{-1} at T_m = 239 K for 20, 40 and 60 nm thick film, respectively. We note that the maximum TCR value increases by increasing the film thickness from 20 to 60 nm. These TCR values are indeed encouraging for further integration in bolometric application. Our TCR values are much larger than those exhibited by LCMO films grown on LAO substrates using PLD process [22]. This is probably due to the annealing temperature which is higher in our case leading to a better film crystallinity and oxygen stoichiometry.

3.3.1. Low temperature behavior ($T < T_P$)

To explain the specific mechanisms of the electrical transport at low temperature in the LCMO films, the resistivity can be fitted using the following formula:

$$\rho(T) = \rho_0 + AT^{\alpha} \quad (1)$$

where ρ_0 is the residual resistivity, A is a free fitting parameter and T^{α} is a generic T-power law which can simulate different scattering processes such as electron–electron (T^2) [23,24], anomalous single magnon (T^3) [25,26] and spin-wave ($T^{7/2}$) [27].

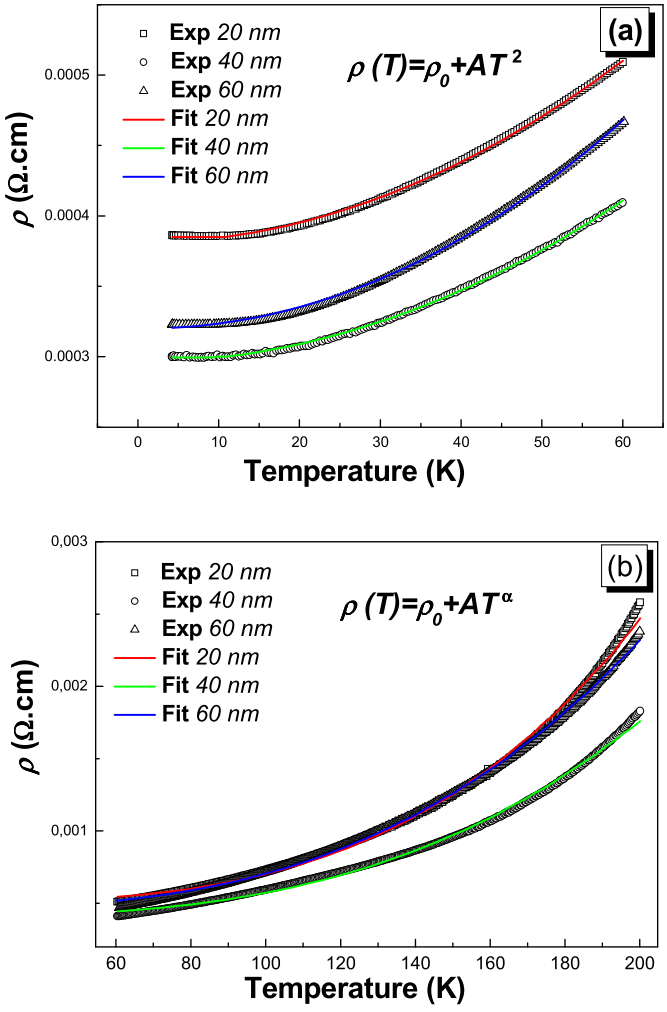

Fig. 5. Temperature dependence of the resistivity for LCMO films (20, 40 and 60 nm) in the metallic zone-I (a) and zone-II (b). The solid lines are the best fit to Equation (1).

Fig. 5 shows the temperature dependence of resistivity and the corresponding fits of the LCMO films grown for different thicknesses in two different range of temperature (5–60 K and 60–200 K). For all films, the fit provides an excellent approximation of the experimental data (R^2 very close to 1 where R^2 is the reliability factor). In the first range of temperature (5–60 K) the resistivity (ρ (T) - ρ0) is well described by $T2$ which corresponds to an electron–electron (e – e) scattering process (Fig. 5(a)). Therefore, in this temperature interval, the diffusion process of electron–electron is independent of the film thickness, as well of the strain induced by substrate. These results are in agreement with several previous works [26,28]. For the second interval of temperature (60–200 K), the $\rho(T)$ graph (Fig. 5 (b)) have been fitted using equation (1). The fitting parameters $\rho 0$, A and α for different thicknesses of the LCMO films are summarized in Table 3. In the low temperature interval (zone II) the thinnest LCMO film (20 nm) is characterized by the largest value of α = 3.34 which does not correspond exactly to any one from of the specific scattering mechanisms cited above. In fact, this value is found between 3 and 3.5 corresponding probably to the diffusion process of anomalous single magnon [25,26] and spin-wave scattering process [27], respectively. Therefore, the conduction mechanism probably corresponds to an increase in the anomalous single magnon scattering involving the spin-wave scattering. As the film thickness increase to 40 then 60 nm, we noted an obvious decrease in the value of α = 3.05–3 to 2.95–3, respectively. For both LCMO films (40 and 60 nm), α is nearly equal to 3, therefore the transport mechanism is likely dominated by the diffusion process of anomalous single magnon [25,26]. The tiny decrease in the value of α for the 60 nm thick can be correlated to the small degree of strain relaxation as has been previously discussed in structural properties section. In conclusion, the coefficient α appear to be strongly related to the strain-induced by the lattice mismatch between LCMO and LAO substrate.

3.3.2. High temperature behavior ($T > T_P$)

In the $T > T_P$, we will explain the transport properties by two models:

* The small polaron model in adiabatic limit: according to the following formula

$$\rho(T) = ATe^{E_A/K_BT} \quad (2)$$

where A is a free parameter, EA is the thermal activation energy and K_B is the Boltzmann constant. This model characterize the polaron hopping process in uniform system (same energy for all sites, equivalent coupling strength for electron-lattice or hole lattice) [29,30].

* Although, the variable Range hopping (VRH) model is described as follows:

$$\rho(T) = \rho_0 exp\left(\frac{T_0}{T}\right)^{1/4} \quad (3)$$

where, $\rho 0$ is the residual resistivity and T_0 is the characteristic VRH temperature. This model is considered to understand the electron

Table 3
Fitting parameters of the ρ (T) at low temperature [60–200 K] for the LCMO films deposited on LAO substrates.

Thickness	20 nm	40 nm	60 nm
ρ_0*10^{-4} (Ω cm)	5.1	4.1	4.7
A*10^{-10}	0.402	1.3	3
α	3.34 ± 0.01	3.05 ± 0.01	2.95 ± 0.01

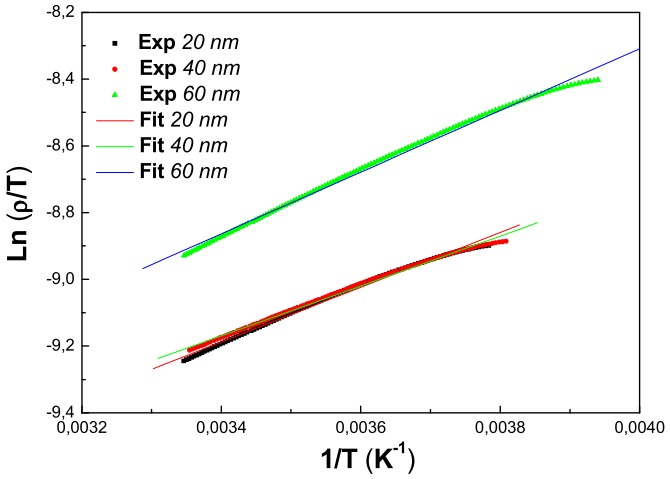

Fig. 6. Ln (ρ/T) versus 1/T and the corresponding fits using the Arrhenius equation at high temperature ($T > TP$) for the LCMO films grown on LAO substrates.

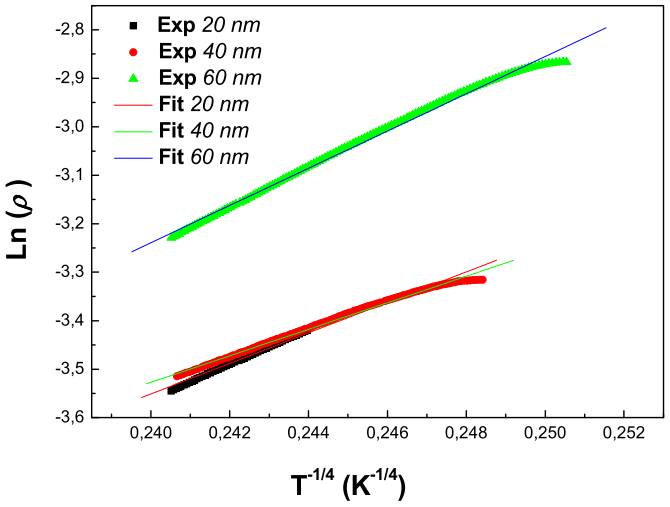

Fig. 7. Ln(ρ) versus $T^{-1/4}$ and the corresponding linear fit for the 20, 40 and 60 nm thick LCMO films above the T_P.

conduction in transport properties [30].

a) Small -polaron Model

The dependence on inverse temperature of Ln(ρ/T) and the corresponding fit using equation (2) at high temperature ($T > TP$) are shown in Fig. 6. For all films, the fit provides an excellent approximation of the experimental data (R^2 very close to 1). The fitting parameters deduced from this simulation are summarized in Table 4. The activation energy *EA* of the 20 nm thin film is *EA*~ 71 meV. The EA value decreases with increasing the film thickness to 40 nm (*EA*~ 64.5 meV). This reduce has been explained in terms of the magnetic disorder caused by interfacial phase separation, localized chemical non-stoichiometry and oxygen vacancies [20]. As discussed earlier, the 40 nm thin film has undergone partial relaxation caused by increasing the thickness. The strain relaxation in the LCMO film generates interfacial misfit dislocations as has been previously reported by means of high resolution transmission electron microscopy observations for the 40 nm thick film grown on LAO substrate [15]. By increasing the film thickness to 60 nm, we note that the activation energy remarkably increases to reach 80 meV. This increase in the value of *EA* is mainly due to the strain relaxation. In fact the 60 nm thick film is more relaxed, in comparison with the 40 nm thick film, however its activation energy is still relatively small in comparison with that of the bulk LCMO (*EA,bulk* ~ 115 meV) [31,32].

b) Variable range hopping (VRH) Model

Fig. 7 shows the experimental *T-1/4*-dependence of Ln(ρ) above *TP* and the corresponding best linear fit using the Mott's model (equation (3)). In Table 5 was summarized the parameters T_0 and $\rho 0$ deduced from the fits. The T_0 values were found to be 9.81 × 105, 5.61 × 105 and 27.8 × 105 K for the 20, 40 and 60 nm thick LCMO films, respectively. Hence, with increased film thickness from 20 to 40 nm, the characteristic of variable range hopping (VRH), temperature (T_0), decreases. This decrease is probably due to the appearance of interfacial phase separation and oxygen vacancies. Then T_0 value drastically increases from 5.61 × 105 K for the 40 nm thick films to reach 27.8 × 105 K for the 60 nm thick film. It can be concluded here that the small degree of strain relaxation induces a notable increase in the characteristic VRH temperature (T_0).

To calculate the localization length ($1/\alpha$), we used the modified formula proposed by Viret et al. [30]. They have proposed that in case of manganites with x = 0.3 divalent cation doping at the rare earth site, the random potential of magnetic origin causes the carrier localization above T_C. This potential is due to the Hund's rule coupling $-J_H \vec{S_i} \cdot \vec{S_j}$ between localized Mn t2g ion cores (S = 3/2) and spins of eg electrons in the conduction band. The localization length ($1/\alpha$) expression is given by $\frac{1}{\alpha} = \left(\frac{171 U_m V}{K_B T_0}\right)^{1/3}$. Where $U_m = 3\frac{J_H}{2}$ is the splitting between the spin-up and spin-down eg bands. In this case (x = 0.3), Um ≈ 2 eV was extracted from optical spectra [33]. V is the unit cell volume per Mn ion, T_0 is the characteristic VRH temperature and *KB* is the Boltzmann constant. Substituting the value of *Um* and *KB*, the above formula becomes: $\frac{1}{\alpha} = \left(\frac{3.965 10^6 V}{T_0}\right)^{1/3}$.

Hence, the average nearest-neighbour hopping distance (R) is given by:

$$R = \left(\frac{9}{8\pi N(E) k_B T}\right)^{1/4}$$

Where *N*(*E*) is the density of available states in the random potential regime of Viret et al. [30] and the value estimated by them

Table 4
Fitting parameters of the $\rho(T)$ at high temperatures using the small polarons model for the LCMO films deposited on LAO substrates.

Thickness	20 nm	40 nm	60 nm
A^*10^{-6}	6.28	8.21	6.14
E_A (meV)	70.69 ± 0.55	64.35 ± 0.40	79.63 ± 0.47

Table 5
Fitting parameters of the ρ (T) at high temperatures using VRH model for the LCMO films deposited on LAO substrates.

LCMO/LAO	20 nm	40 nm	60 nm
$T_0{}^*10^5$(K)	9.81 ± 0.001	5.61 ± 0.002	21.79 ± 0.003
$\rho_0{}^*10^{-6}$ (Ω cm)	15.11 ± 0.01	17.56 ± 0.01	3.88 ± 0.01
1/α (Å)	6.14 ± 0.43	7.41 ± 0.17	4.71 ± 0.10
R (Å) for H = 3T	17.61 ± 0.02	18.42 ± 0.02	16.61 ± 0.02

for LCMO is $N(E) = 9 \times 10^{26}$ m^{-3} eV^{-1}, the above expression becomes:

$$R = \left(\frac{4.6112x10^{-24}}{\alpha T}\right)^{1/4}$$

The calculated values of the localization length ($1/\alpha$) are found to be 6.14, 7.41 and 4.71 Å for the 20, 40 and 60 nm thick LCMO films, respectively. Furthermore the calculated values of the average hopping distance (R) are 17.61, 18.42 and 16.61 Å for 20, 40 and 60 nm LCMO thin film, respectively. From these results, we can obviously conclude that the magnetic disorder causes an increase in the value of ($1/\alpha$) so a decrease in the value of T_0 namely the carriers becomes unconfined which comes in turn raises of the R value. As well, the small degree of strain relaxation (from 40 to 60 nm) is the reason of reducing the localization length ($1/\alpha$) value therefore the evolution of T_0, that is the carriers becomes more localized so the decrease of R value.

3.3.3. Magnetoresistive properties

The temperature dependence of resistivity graphs for 20, 40 and 60 nm films at different applied magnetic field (1, 2, 3, 5 and 7 T) are shown in Fig. 8. All films exhibit paramagnetic to ferromagnetic transition for various applied magnetic fields. By increasing the magnetic field, the electrical resistivity drops quite sharply. In the presence of an external applied magnetic field, the magnetic polaron becomes fluctuating and then the decrease in the resistivity. Which also can be explain by the coexistence of FM and PI phase in short range of paramagnetic region [34].

The magnetoresistance (MR) was calculated from the relation: $MR = [[\rho(0)\text{-}\rho(H)]/\rho(0)] \times 100$, where $\rho(0)$ and $\rho(H)$ are the values of resistivity in the absence and in presence of a magnetic field, respectively. For different applied magnetic field (1, 2, 3, 5 and 7 T), the MR of the LCMO/LAO thin films was measured in the different temperature range (5–300 K) for 1 and 7 T, and (150–300 K) for 2, 3 and 5 T. The corresponding data are plotted in Fig 9 (not all shown), showing obviously an increase in the MR (%) by increasing the magnetic field and the film thickness. The maximum values of the MR (%) values are obtained at a temperature close the Curie temperature (T_C). The best MR (~91%) was observed for 60 nm thick at H = 7 T and T = 248 K, and the lowest MR (39%) was found for the 20 nm thick at $H = 1$ T and $T = 251$ K.

3.3.4. Resistive switching properties

The measured resistive switching hysteresis loop (RSHL) on the 80 nm LCMO film with Ag electrodes are shown in Fig. 10. Two distinctive states of resistance can be observed, that could be exploited as two distinct states for a memory device. Repeatable values were obtained after two loops, which remain stable at least for several hours. A change of resistance between these two states of approximately 15% was found. The fact that the resistance of the junction is reduced by applying positive pulses and recovered by applying negative pulses of different amplitude indicates a resistive switching of the bipolar type, in accordance to what is expected for devices based on metal/complex oxides, where the resistive switching mechanism is associated with the electromigration of oxygen vacancies [35].

4. Conclusion

In summary, the film thickness and the induced strain effects on the structural and physical properties of the epitaxial LCMO films grown on LAO substrates have been investigated. The evolution of

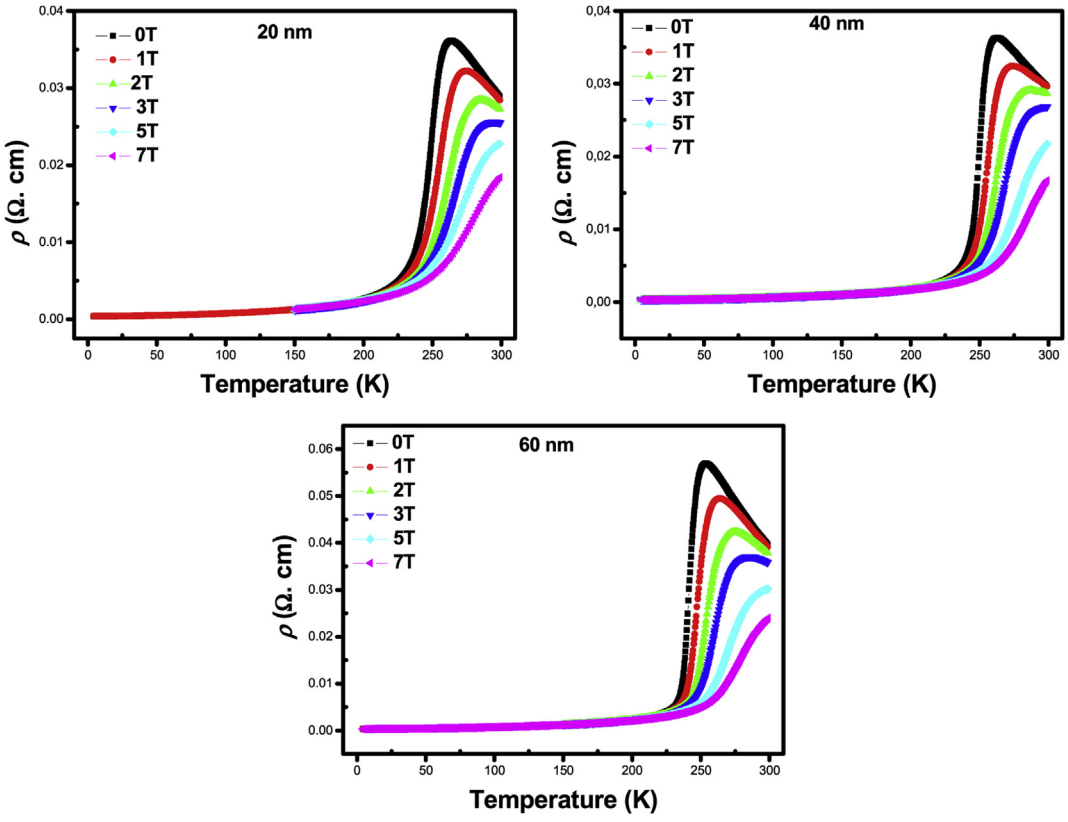

Fig. 8. Resistivity variation as a function of temperature of the 20, 40 and 60 nm thick LCMO films at different magnetic field.

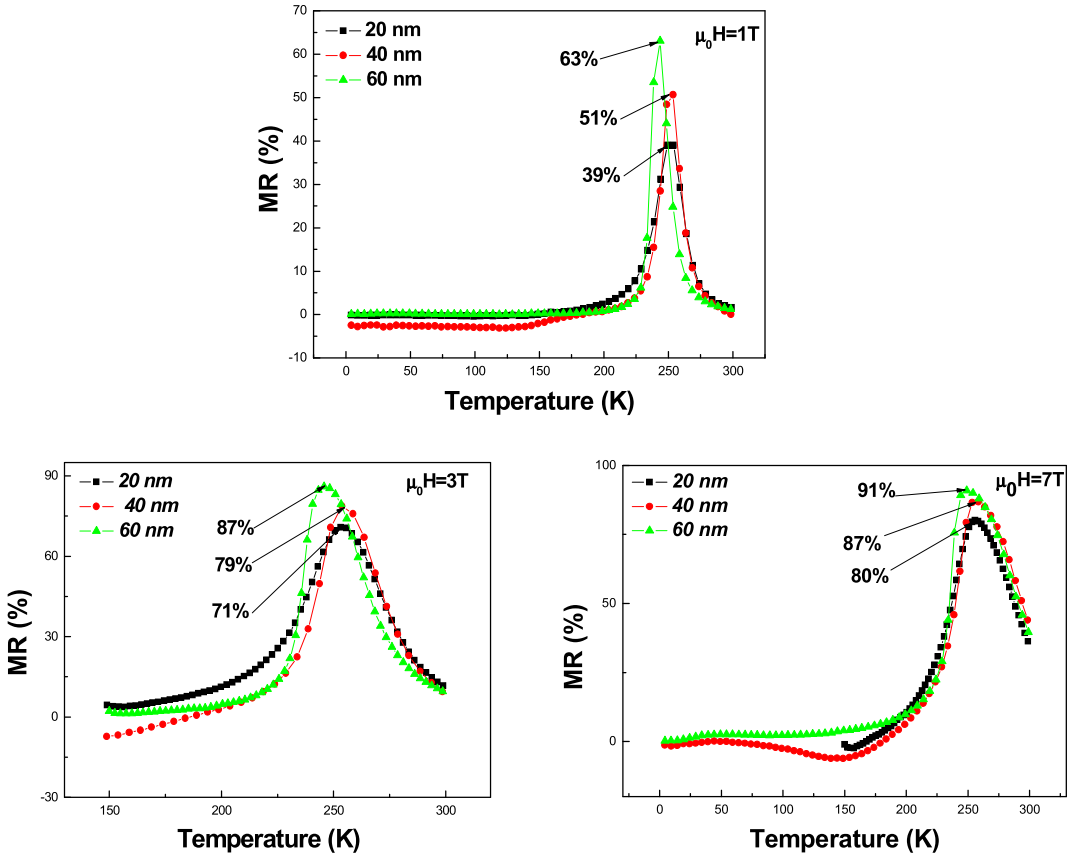

Fig. 9. The temperature dependence of MR for $La_{0.7}Ca_{0.3}MnO_3$ films at different magnetic field: 1, 3and 7 T.

the structural properties such as the cell parameters and lattice strain have been studied using XRD analysis. We observe that an increase of the thickness from 20 to 60 nm induces an important strain relaxation which in turn influences the transport and magnetic behavior of the LCMO film. The Curie temperature (T_C) and the transport mechanisms in different temperature ranges for different film thicknesses have been correlated to the structural properties. The LCMO films exhibit good physical properties such high *TCR*, large MR and RSHL making them excellent candidate for bolometric, magnetic and memory devices.

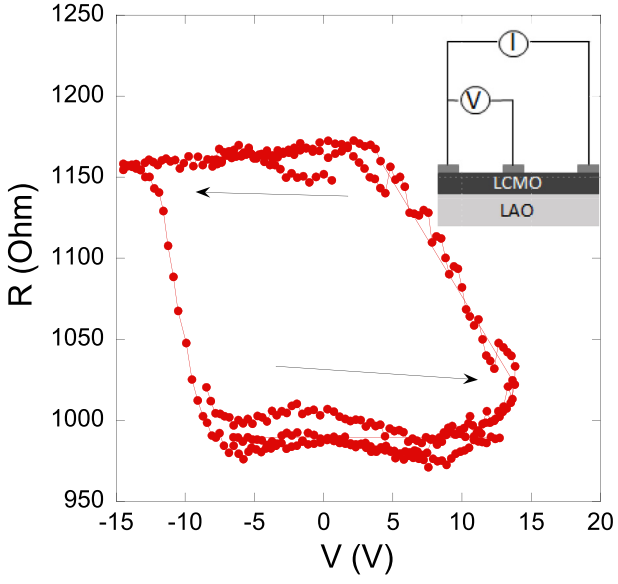

Fig. 10. RSHL measurements showing the remnant resistance of the LCMO/Ag junction as a function of the voltage amplitude of a previously applied 10 ms electric pulse. The measurement was performed using a bias current Ib = 0.5 mA. The inset shows the contact configuration used for the remnant resistance measurement.

Acknowledgments

The authors would like to thank Dr. Sobhi Hcini from the University of Monastir, Tunisia for the faithful discussions and help in the fitting of the temperature dependence of the resistivity graphs.

References

[1] S. Jin, T.H. Tiefel, M. Mc Cormack, R.A. Fastnacht, R. Ramesh, L.H. Chen, Science 264 (1994) 413.
[2] R.V. Helmolt, J. Weeker, B. Holzapfel, L. Schultz, K. Samwer, Phys. Rev. Lett. 71 (1993) 2331.
[3] C.H. Chen, S.-W. Cheong, Phys. Rev. Lett. 76 (1996) 4042.
[4] Z. Jirak, F. Damay, M. Hervieu, C. Martin, B. Raveau, G. Andreé, F. Boureé, Phys. Rev. B 61 (2000) 1181.
[5] Y. Okuda, Y. Tomioka, A. Asamitsu, Y. Tokura, Phys. Rev. B 61 (2000) 8009.
[6] Y. Tokura, Rep. Prog. Phys. 69 (2006) 797.
[7] K. Daoudi, T. Tsuchiya, T. Kumagai, Thin Solid Films 516 (2010) (2008) 6325.
[8] A.M. Haghiri-Gosnet, J.P. Renard, J. Phys. D Appl. Phys. 36 (2003) R127.
[9] A. Sawa, Mater. Today 11 (2008) 28.
[10] C. Acha, M.J. Rozenberg, J. Phys. Condens. Matter 21 (2009) 045702.
[11] O. Chmaissem, B. Dabrowski, S. Kolesnik, J. Mais, J.D. Jorgensen, S. Short, C.E. Botez, P.W. Stephens, Phys. Rev. B 72 (2005) 104426.
[12] O.I. Lebedev, G. van Tendeloo, S. Amelinckx, B. Leibold, H.-U. Habermeier, Phys. Rev. B 58 (1998) 8065.
[13] I.T. Serenkov, V.I. Sakharov, Y.A. Boikov, V.A. Danilov, M.P. Volkov, T. Claeson, J. Phys. B 404 (2009) 5234.
[14] S. El Helali, K. Daoudi, A. Fouzri, M. Oumezzine, M. Oueslati, T. Tsuchiya, Appl. Phys. A 108 (2012) 379–384.

[15] K. Daoudi, T. Tsuchiya, S. Mizuta, I. Yamaguchi, T. Manabeand, T. Kumagai, J. Appl. Phys. 98 (013507) (2005).
[16] A. de Andres, J. Rubio, G. Castro, S. Taboada, J.L. Martinez, J.M. Colino, Appl. Phys. Lett. 83 (2003) 713.
[17] M. Bibes, Ll Balcells, S. Valencia, J. Fontcuberta, M. Wojcik, E. Jedryka, S. Nadolski, Phys. Rev. Lett. 87 (067210) (2001).
[18] J.C. Debnath, J.H. Kim, Y. Heo, A.M. Strydom, S.X. Dou, J. Appl. Phys. 113 (2013) 063508.
[19] C.J. Lu, Z.L. Wang, C. Kwon, Q.X. Jia, J. Appl. Phys. 88 (2000) 4032.
[20] R. Prasad, H.K. Singh, M.P. Singh, W. Prellier, P.K. Siwach, Armarjeet Kaur, J. Appl. Phys. 103 (2008) 08396.
[21] M. Bibes, S. Valencia, L. Balcells, B. Martınez, J. Fontcu-berta, M. Wojcik, S. Nadolski, E. Jedryka, Phys. Rev. B 66 (2002) 134416.
[22] A. Goyal, M. Rajeswari, R. Shreekala, S.E. Lofland, S.M. Bhagat, T. Boettcher, C. Kwon, R. Ramesh, T. Venkatesan, Appl. Phys. Lett. 71 (1997) 2535.
[23] A. Urushibara, Y. Moritomo, T. Arima, A. Asamitsu, G. Kido, et Y. Tokura, Phys. Rev. B 51 (1995) 14103.
[24] G.J. Snyder, R. Hiskes, S. DiCarolis, M.R. Beasley, et T.H. Geballe, Phys. Rev. B 53 (1996) 14434.
[25] T. Akimoto, Y. Moritomo, A. Nakamura, N. Furukawa, Phys. Rev. Lett. 85 (2000) 3914.
[26] S. Mercone, C.A. Perroni, V. Cataudella, C. Adamo, M. Angeloni, C. Aruta, G. De Filippis, F. Miletto, A. Oropallo, P. Perna, A. Yu Petrov, U. Scotti di Uccio, L. Maritato, Phys. Rev. B 71 (2005) 064415.
[27] X.J. Chen, H.U. Habermeier, C.L. Zhang, H. Zhang, C.C. Almasan, Phys. Rev. B 67 (2003) 134405.
[28] M.B. Salamon, M. Jaime, Rev. Mod. Phys. 73 (2001) 583.
[29] D. Emin, T. Holstein, Ann. Phys. Paris. 53 (1969) 439.
[30] M. Viret, L. Ranno, J.M.D. Coey, Phys. Rev. B 55 (1997) 8067.
[31] M.E. Hawley, C.D. Adams, P.N. Arendt, E.L. Brisha, F.H. Garzon, R.J. Houlton, M.F. Hundley, R.H. Heffner, Q.X. Jia, J. Neumeier, X.D. Wu, J. Cryst. Growth 174 (1997) 455.
[32] M. Jain, E. Bauer, F. Ronning, M.F. Hundley, L. Civale, H.Y. Wang, B. Maiorov, A.K. Burrell, T.M. McClesky, S.R. Foltyn, R.F. DePaula, Q.X. Jia, J. Am. Ceram. Soc. 91 (2008) 1858.
[33] Y. Okimoto, T. Katsufuji, T. Ishikawa, A. Urushibara, T. Arima, Y. Tokura, Phys. Rev. Lett. 75 (1995) 109.
[34] M. Uehara, S. Mori, C.H. Chen, S.-W. Cheong, Nat. Lond. 399 (1999) 560.
[35] M.J. Rozenberg, M.J. Sánchez, R. Weht, C. Acha, F. Gomez-Marlasca, P. Levy, Phys. Rev. B 81 (2010) 115101.